Structure
Article

Nucleotides and Substrates Trigger the Dynamics of the Toc34 GTPase Homodimer Involved in Chloroplast Preprotein Translocation

Christina Lumme,[1,9,10] Hasret Altan-Martin,[2,9] Reza Dastvan,[3,5,7,8,9] Maik S. Sommer,[2] Mislav Oreb,[1,11] Denise Schuetz,[3,5,7] Björn Hellenkamp,[1] Oliver Mirus,[2] Jens Kretschmer,[2,14] Sevdalina Lyubenova,[3,5,7,12] Wolfgang Kügel,[4] Jan P. Medelnik,[2,13] Manuela Dehmer,[2] Jens Michaelis,[4] Thomas F. Prisner,[3,5,7] Thorsten Hugel,[1] and Enrico Schleiff[2,5,6,*]

[1]Physics Department E22 and IMETUM, Technical University Munich, 85748 Garching, Germany
[2]Institute of Molecular Cell Biology of Plants, Goethe University, 60438 Frankfurt, Germany
[3]Institute of Physical and Theoretical Chemistry, Goethe University, 60438 Frankfurt, Germany
[4]Physics Department, Ulm University, 89081 Ulm, Germany
[5]Cluster of Excellence "Macromolecular Complexes", Goethe University, 60438 Frankfurt, Germany
[6]Center for Membrane Proteomics, Goethe University, 60438 Frankfurt, Germany
[7]Center for Biomolecular Magnetic Resonance, Goethe University, 60438 Frankfurt, Germany
[8]Department of Molecular Physiology & Biophysics, Vanderbilt University, 741 Light Hall, 2215 Garland Avenue, Nashville, TN 37232, USA
[9]These authors contributed equally to this work
[10]Present address: XLAB Göttingen, 37077 Göttingen, Germany
[11]Present address: Molecular Physiology and Genetics of Lower Eukaryotes, Goethe University, 60438 Frankfurt, Germany
[12]Present address: Business Unit EPR/Sales & Applications, Bruker BioSpin GmbH, 76287 Rheinstetten, Germany
[13]Present address: Center for Regenerative Therapies Dresden (CRTD), Cluster of Excellence, Technical University of Dresden, 01307 Dresden, Germany
[14]Present address: Center for Biochemistry and Molecular Cell Biology, Medical Department, Göttingen University, 37073 Göttingen, Germany
*Correspondence: schleiff@bio.uni-frankfurt.de
http://dx.doi.org/10.1016/j.str.2014.02.004

SUMMARY

GTPases are molecular switches that control numerous crucial cellular processes. Unlike bona fide GTPases, which are regulated by intramolecular structural transitions, the less well studied GAD-GTPases are activated by nucleotide-dependent dimerization. A member of this family is the translocase of the outer envelope membrane of chloroplast Toc34 involved in regulation of preprotein import. The GTPase cycle of Toc34 is considered a major circuit of translocation regulation. Contrary to expectations, previous studies yielded only marginal structural changes of dimeric Toc34 in response to different nucleotide loads. Referencing PELDOR and FRET single-molecule and bulk experiments, we describe a nucleotide-dependent transition of the dimer flexibility from a tight GDP- to a flexible GTP-loaded state. Substrate binding induces an opening of the GDP-loaded dimer. Thus, the structural dynamics of bona fide GTPases induced by GTP hydrolysis is replaced by substrate-dependent dimer flexibility, which likely represents a general regulatory mode for dimerizing GTPases.

INTRODUCTION

Guanosine triphosphate (GTP) binding and G proteins are molecular switches for the regulation of numerous cellular processes (Wittinghofer and Vetter, 2011). For instance, in plants, they are involved in the regulation of symbiotic interactions (Yuksel and Memon, 2009), cell polarity signaling (Yang, 2008), vesicle transport (Hwang and Robinson, 2009), plastid division (Yoshida et al., 2012), and plastid protein translocation (Sommer and Schleiff, 2009). In all of these processes, guanosine triphosphatases (GTPases) serve as transducers of information by their ability to hydrolyze GTP, triggering structural transitions sensed by G protein-specific effectors (Gasper et al., 2009). The nucleotide cycle of bona fide GTPases is generally controlled by GTPase-activating proteins (GAPs) and guanine exchange factors (GEFs) (Bos et al., 2007; Scheffzek et al., 1998). GAPs complement or stabilize the catalytic center of the GTPase, thereby increasing GTP hydrolysis by several orders of magnitude. GEFs reduce the nucleotide affinity promoting the nucleotide exchange. In some cases, nucleotide release is regulated by guanosine diphosphate (GDP) dissociation inhibitors (GDIs) and GDI displacement factors (GDFs) (DerMardirossian and Bokoch, 2005). The provoked structural change between the GTP and GDP states ensures high-affinity interactions with effectors in the GTP form, in which two dynamic structural elements coordinating the γ-phosphate of the GTP (switches I and II) relax after GTP hydrolysis and release of the inorganic phosphate (Wittinghofer and Vetter, 2011).

G proteins have been classified according to their mode of function. One subgroup unifies the G proteins activated by nucleotide-dependent dimerization (GADs), which are able to form (pseudo)homodimers (Gasper et al., 2009). GADs possess all structural elements for the canonical switch mechanism of bona fide G proteins but reciprocally complement their catalytic sites in the dimeric state, rendering the presence of classical GAPs

unnecessary (Wittinghofer and Vetter, 2011). The high nucleotide exchange rate, a consequence of their low nucleotide affinity, makes them independent of GEFs as well (Gasper et al., 2009).

GADs are involved in numerous fundamental cellular functions. Important examples are membrane fusion and fission factors such as atlastin (Bian et al., 2011), dynamin (Chappie et al., 2010; Ford et al., 2011), and septin (Oh and Bi, 2011); the tRNA-modifying protein MnmE (Meyer et al., 2009), Xab1 (involved in DNA repair) (Gras et al., 2007; Nitta et al., 2000); and the signal recognition particle (SRP) and its receptor (SR) (Focia et al., 2004). The latter belong to the signal recognition GTPases and MinD and BioD (SIMIBI) superclass (Leipe et al., 2002).

A further example of a plant-specific GAD is the G protein Toc34, a member of the translation factor (TRAFAC)-related superclass (Leipe et al., 2002). Toc34 is the main receptor of the preprotein translocon of the outer envelope of chloroplasts (TOC), by which almost 95% of all chloroplast proteins are post-translationally imported into the organelle (Schleiff and Becker, 2011). The GTPase cycle of Toc34 is thus thought to be the major regulatory circuit of translocation and thereby chloroplast protein import and organelle development per se (Sommer and Schleiff, 2009). Recently, the transition between different isoforms of Toc34 has been discussed as a major regulatory circuit to redirect substrate specificity (Ling et al., 2012). This discussion has emphasized the importance of this receptor family.

Toc34 forms homodimers in vitro and in the crystal lattice (Bionda et al., 2008; Koenig et al., 2008; Sun et al., 2002). Dimerization is mediated by specific conserved residues within the G domain and is abrogated upon their mutation (Reddick et al., 2007). Accordingly, plants expressing the arginine 133 to an alanine variant of Toc34, show both reduced dimerization capacity and reduced import efficiency. This suggests functional relevance of homodimerization in vivo (Aronsson et al., 2010). The dimerization interface covers the nucleotide-binding site (Koenig et al., 2008; Sun et al., 2002), and preprotein binding interferes with homodimerization by an unknown mechanism (Oreb et al., 2011). Additionally, Toc34 engages heterodimeric conformations by interaction with the second receptor GTPase of the TOC, Toc159 (Bauer et al., 2002; Becker et al., 2004).

Although established in vitro, the consequences of homo- and heterodimer formation for the function and the GTPase cycle of TOC remain elusive (Sommer and Schleiff, 2009). It has been assumed that dimerization provides a reciprocal GAP function, given that the arginine 133 reaches from one protomer into the catalytic center of the other in the position of the β-phosphate of the nucleotides (Sun et al., 2002), as does the arginine finger of Ras/Rho GAPs (Scheffzek et al., 1998). In contrast, GTP hydrolysis is not accelerated upon homodimer formation, and therefore the need for a co-GAP complementing the catalytic site has been postulated (Koenig et al., 2008). The GDP and GTP forms of Toc34 show only marginal conformational differences in the crystal structures (Koenig et al., 2008; Sun et al., 2002), an observation that is unexpected, because structural changes in G proteins are typically regulatory switches.

We reanalyzed the structural flexibility of the Toc34 homodimer by bulk and single-molecule Förster resonance energy transfer (FRET) (Roy et al., 2008) and pulsed electron-electron double-resonance (PELDOR or DEER) spectroscopy (Milov et al., 1984; Schiemann and Prisner, 2007) for the following reasons: (1) the importance of Toc34 for proper TOC function and therefore chloroplast function and biogenesis per se, (2) the limited knowledge of the regulation of Toc34 and GAD-type GTPases in general, and (3) the still very limited understanding of the molecular details of the mechanism of translocation via TOC. We report that both the nucleotide loading state and preprotein binding modulate dimer conformation. We demonstrate the existence of significant flexibility of the dimeric conformation that was not seen in the crystal structures and that preprotein binding causes an opening of the dimer. Thus, we uncovered an unexpected substrate-induced mode of GAD regulation, which explains the dependence of Toc34 function on both nucleotides and dimerization.

RESULTS

The Homodimeric State of *ps*Toc34 Exists in Native Membranes

Toc34 is thought to engage in a homodimeric conformation, at least in vitro. To show the Toc34 homodimer within the TOC complex in its native environment, *ps*Toc34 full-length variants ($Toc34_{FL}$) exposing a single cysteine residue were translated in the presence of ^{35}S methionine and a chemically modified, benzophenone-loaded cysteine tRNA (BP-S-Cys-$tRNA^{Cys}$). The proteins were generated in a cysteine-free background with the intrinsic cysteine at position 215 being substituted to serine (C215S). Glutamine 34 and aspartate 203 were chosen as controls because of their distance from the dimeric interface (Figure 1A). Serine 66 is in close proximity to inset I4 of the other protomer in the dimer, whereas aspartate 219 could reach toward the other protomer, assuming a certain flexibility of inset I6 (Sun et al., 2002) (Figures S1A and S1B available online). The proteins were imported into isolated pea chloroplasts. Proper insertion was confirmed by extraction with high salt (exemplified in Figure 1B). Assembly into the TOC_{core} complex was verified by native PAGE after repurification of organelles (Ladig et al., 2011) (Figure 1C).

We observed two distinct crosslinking adducts migrating at ~66 kDa and ~120 kDa after stabilization of physical interactions by UV crosslinking. Additionally, a nonspecific product (*) considerably higher than 120 kDa also present in the cysteine 215 to serine mutant was found (Figures 1D and S1). Considering the composition of the TOC_{core} complex (Kikuchi et al., 2006; Schleiff et al., 2003) and the given molecular weight of Toc34 (34 kDa), the 66 kDa product most likely represents a Toc34 homodimer. This is consistent with findings using in organello crosslinking with copper(II)-1,10-phenanthroline (Lee et al., 2009) and demonstrates the ability of specific homodimer formation in a "face-to-face" conformation as suggested by the crystal structures. Considering the molecular weights of Toc75 and Toc159 (75 kDa and the 86 kDa degradation products of Toc159, respectively) and the cytosolic exposure of the soluble domain of Toc75 (Sommer et al., 2011), the larger adduct can be assigned as either a Toc75-Toc34 or a Toc159-Toc34 heterodimer, a determination that deserves closer study.

Homodimerization Does Not Interfere with Toc34 GTPase Activity

We investigated the conformational freedom of the G domain in the homodimer of Toc34 by PELDOR and FRET analyses in vitro.

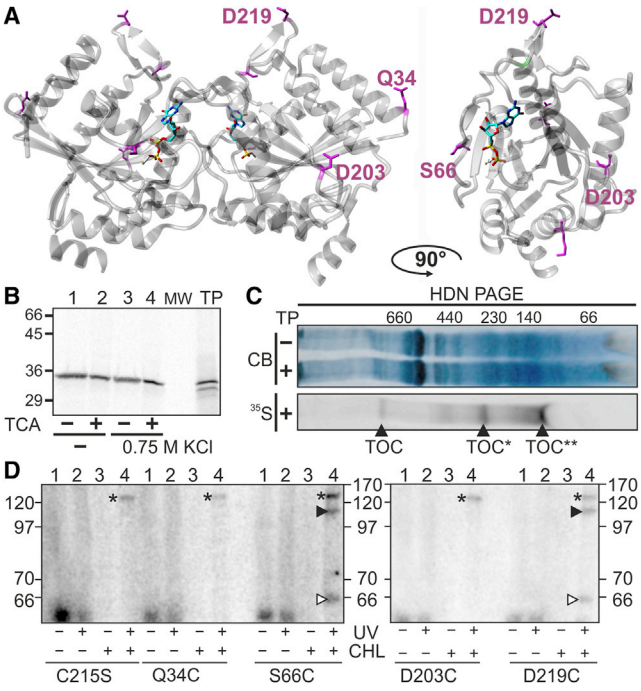

Figure 1. Toc34 Dimerizes in Endogenous Membranes

(A) Side view of the dimeric G domains (left) or the dimer interface (right) of *ps*Toc34 indicating the positions of the cysteines introduced for crosslinking (purple).

(B) ^{35}S-labeled *ps*Toc34 (*ps*Toc34$_{FL}$) was incubated with pea chloroplasts. Chloroplasts were reisolated (lane 1) with or without washing with high salt (lane 3). Lanes 2 and 4 confirm trichloroacetic acid (TCA) precipitation efficiency. TP: 10% of translation product as input control.

(C) After import of *ps*Toc34, chloroplasts were subjected to high-definition native (HDN)-PAGE. The migration of *ps*Toc34$_{FL}$ (▲) with the holo-TOC$_{core}$ complex (~750 kDa) and the TOC$_{core}$ complex intermediates (*,**) is indicated as established previously (Ladig et al., 2011).

(D) Wild-type or indicated mutants of *ps*Toc34$_{FL}$ translated in the presence of modified tRNA (lane 1; lane 2 after UV treatment) were imported into chloroplasts (lane 3). Organelles were treated with UV light, washed with high salt, and proteins precipitated by TCA (lane 4). Crosslinks to Toc34, ► putative crosslinks to the 86 kDa degradation fragment of Toc159 or Toc75. *Nonspecific crosslinking product present in all samples. The Coomassie Brilliant Blue-stained PAGE image is shown in Figure S1. CHL, chloroplasts. See also Figure S1.

The two complementary methods offer the opportunity to monitor structural changes in the nanometer range. In terms of PELDOR, distances up to 8 nm can be measured, depending on the accessible observation time window (Schiemann and Prisner, 2007). In FRET analysis, distances up to 10 nm are detectable, depending on the dye pair used (Roy et al., 2008). We generated a construct series to achieve a stable homodimer of the Toc34 G domain, which in vivo is tethered to the TOC complex via its C-terminal transmembrane domain. We used the coiled-coil-forming leucine zipper of kinesin-1 (*dm*KHC) from *Drosophila melanogaster* either directly fused to the G domain (Toc34$_Z$) (Figure S2) or with a short non-coiled-coil-forming spacer in between to link up two *ps*Toc34 monomers to a stable dimer (Toc34$_{SZ}$) (Figure 2A). The latter likely reflects the native C-terminal membrane anchoring of Toc34 (Figure S2). Multiple single amino acid substitutions to cysteines were introduced in the cysteine-free C215S variant (for the sake of simplicity, not further mentioned) for subsequent studies (Figure 2A).

As previously shown, all proteins were recombinantly expressed and purified in a GDP-loaded state (Koenig et al., 2008). The purified proteins are homodisperse and migrate exclusively as dimers, as determined by analytical size exclusion chromatography (Figure S2). K_M and k_{cat} values for GTP hydrolysis in all wild-type receptors are similar to Toc34$_{\Delta TM}$, confirming that nucleotide recognition and hydrolysis are not significantly affected by zipper-enforced dimerization (Figures 2C and S2; Table 1). Further, we confirmed that experiments can be performed at room temperature (22°C) by analyzing the activity of *ps*Toc34$_{\Delta TM}$ via multiple GTP turnover hydrolysis under rising temperatures, which revealed that the activity remained comparable between 20°C or 30°C (Figure 2D). Consequently, we used *ps*Toc34$_{SZ}$ for the subsequent studies.

Based on the crystal structures of the dimeric *ps*Toc34 G domain (Koenig et al., 2008; Sun et al., 2002), serine 66 (*ps*Toc34$_{SZ}$ S66C), methionine 79 (*ps*Toc34$_{SZ}$ M79C), valine 78 (*ps*Toc34$_{SZ}$ V78C), lysine 143 (*ps*Toc34$_{EC}$ K143C), and aspartic acid 175 (*ps*Toc34$_{SZ}$ D175C) were mutated for labeling at exposed but structurally rigid positions (Figures 2A and 3A). We analyzed the activity of all variants, whereby *ps*Toc34$_{SZ}$ M79C was analyzed representatively for the two adjacent mutants *ps*Toc34$_{SZ}$ M79C and *ps*Toc34$_{SZ}$ V78C. The mutants are functional with slightly higher K_M and k_{cat} values for multiple turnover GTP hydrolysis compared to the wild-type (Figure 2E; Table 1).

The Structural Composition of the Homodimeric Toc34 GTPase

Four variants of *ps*Toc34$_{SZ}$, with single cysteines distributed over the protein from a region close to and a region distant from the lipid bilayer in the native protein, were used to analyze the conformational properties of the dimeric G domain in the GDP-loaded state and without preprotein in fast-frozen solution by PELDOR.

To monitor the interprotomer distances of the dimer in a region close to the lipid bilayer in the native protein, the variant *ps*Toc34$_{SZ}$ K143C was measured (Figure 3B; Table 2). We fitted the obtained background-corrected data by either Tikhonov regularization or a two-Gaussian distance distribution. The direct comparison of the obtained distance distributions justified the assumption of a two-state Gaussian model (Figure S3). Accordingly, we analyzed all subsequent data using a two-state Gaussian model. On the basis of this analysis, we obtained two distance populations (Figure S3), one with 26 ± 6 Å agreeing with the distance in the X-ray structure (1H65) and a second, longer average distance with a very broad distance distribution (55 ± 20 Å).

Next, we analyzed the distances of PELDOR spin labels within variants where the label is in the central region of Toc34 (*ps*Toc34$_{SZ}$ M79C and *ps*Toc34$_{SZ}$ S66C) (Figure 3B; Table 2). For *ps*Toc34$_{SZ}$ M79C, we obtained one population with a distance of 65 ± 1 Å, as expected based on the X-ray structure, and a second population with a broad distance population. As the distance for *ps*Toc34$_{SZ}$ M79C is close to the detection limit of PELDOR under the stated conditions, we confirmed the distance reliability by measuring with enlarged dipolar evolution

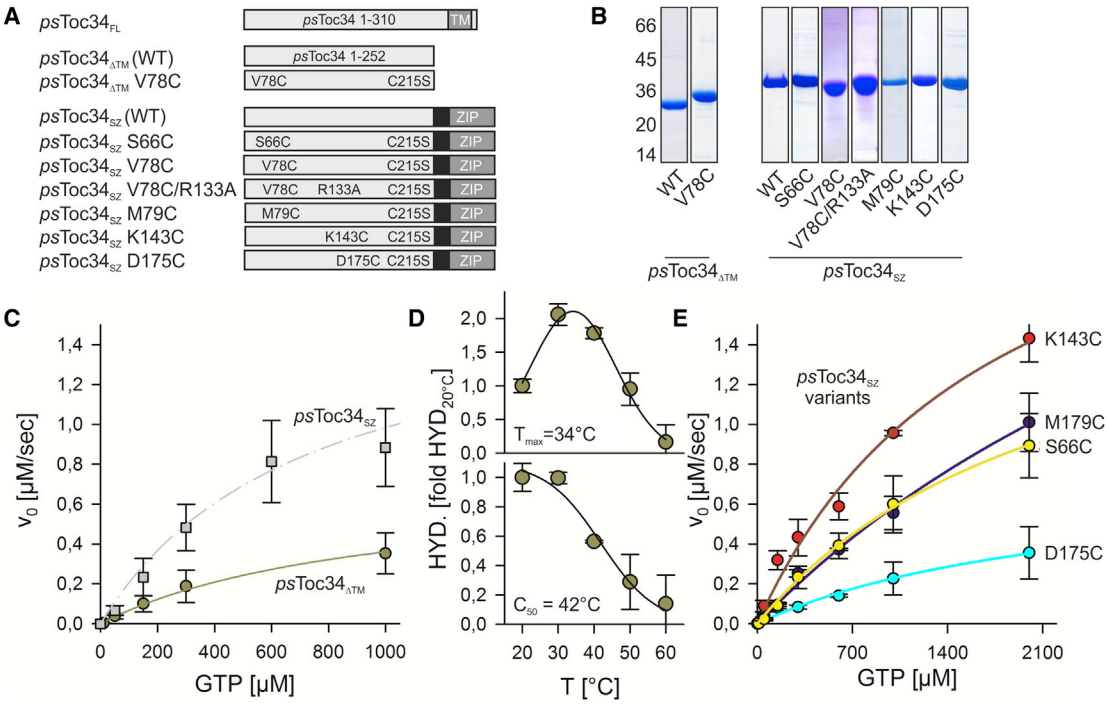

Figure 2. The Bulk Properties of Toc34 Variants Used in This Study

(A) The constructs used in this study are shown as a bar diagram indicating the names used throughout the paper and the point mutations introduced. The G domain of *ps*Toc34 is in light gray, the leucine zipper is in dark gray, and the non-coiled-coil spacer is in black.

(B) The heterologously expressed proteins and their purity after affinity chromatography are shown. The nucleotide loading state was confirmed by thin-layer chromatography (not shown).

(C) The Michaelis-Menten kinetics for GTP hydrolysis were determined. The solid line indicates the least squares fit analysis to the Michaelis-Menten equation, and the gray dashed line shows extrapolations for comparison. The initial rates were determined and the kinetics were analyzed by using a classical Michaelis-Menten equation.

(D) To test the thermosensitivity of *ps*Toc34$_{\Delta TM}$, multiple turnover hydrolysis (HYD) was performed at the indicated temperatures. The heat recovery efficiency of *ps*Toc34$_{\Delta TM}$ was probed by determination of the hydrolytic activity 1 hr after preincubation of the protein at different temperatures (top). The rate of multiple turnover hydrolysis of *ps*Toc34$_{\Delta TM}$ at different temperatures was normalized to the rate observed at 20°C. The least squares fit analysis to a Gaussian distribution (line) is shown. The rate of multiple turnover hydrolysis of *ps*Toc34$_{\Delta TM}$ was analyzed at 20°C after preincubation of the protein for 30 min at the indicated temperatures (bottom). The mean ± SD of multiple experiments and the least squares fit analysis of substrate inhibition (line) are shown.

(E) Graph illustrating the Michaelis-Menten kinetics for GTP hydrolysis of the indicated mutants, which were determined as described in (C).

See also Figure S2.

time of 8.2 µs, which yielded identical results (data not shown). In contrast, for *ps*Toc34$_{SZ}$ S66C, only a single distance of 50 Å was observed (Figure 3B, Table 2).

We then measured PELDOR of the *ps*Toc34$_{SZ}$ D175C variant, where the label is positioned most distant from the lipid bilayer (in the native context). We found a single distance of 42 Å, which again is in agreement with the X-ray structure (1H65) (Figure 3B; Table 2). To summarize, the observed main distances are in agreement with the crystal structure and confirm that the monomers are not arranged back-to-back.

In parallel, the time-dependent structural flexibility of the Toc34 homodimer was analyzed by using single-molecule FRET measurements, which monitor changes in the distance between a FRET donor (ATTO 550) and a FRET acceptor (ATTO 647N) attached to the Toc34 homodimer (Figure S4) in real time with nanometer-level accuracy. As a FRET measurement is most accurate around the Förster radius of the FRET pair (65 Å here), we used cysteine mutants at position aspartate 36 or valine 78 (*ps*Toc34$_{SZ}$ V78C) (Figures 2A and 3A).

Using labels positioned at aspartate 36, we did not observe a FRET signal (Table 3) as expected from the distance in the crystal structure (88 Å) and the fluorophore dimension including linker (~10 Å). A FRET signal was expected only in the case of an inverted dimer, and thus the absence of the signal confirmed the correct orientation of the monomers in the dimer according to the crystal structure.

Measuring fluorophore-labeled wild-type *ps*Toc34$_{SZ}$ (labeled at the native cysteine 215) yielded a FRET efficiency of 89%, which corresponds to ~46 Å (Table 3). Considering the dimensions of the fluorophore and the possibility of structural relaxation in solution in comparison to crystal packing (Ratzke et al., 2012), the distance is close to the range expected from the crystal structure (~21 Å). However, the native cysteine is in a very flexible region of the protein (Sun et al., 2002). Therefore, for further measurements, we used the *ps*Toc34$_{SZ}$ V78C variant, where the label is positioned in a more rigid structural environment. Figure 4A shows exemplarily a single molecule fluorescence trace for surface-immobilized GDP-loaded *ps*Toc34$_{SZ}$

Table 1. Multiple Turnover GTP Hydrolysis

Protein[a]	V_{max} (μM/s)	K_M (mM)	k_{cat} (s^{-1})
*ps*Toc34$_{\Delta TM}$	0.6 ± 0.1	0.7 ± 0.1	0.2
*ps*Toc34$_{Z}$	0.7 ± 0.1	0.6 ± 0.1	0.2
*ps*Toc34$_{SZ}$	1.2 ± 0.2	0.7 ± 0.1	0.4
*ps*Toc34$_{SZ}$ S66C	1.9 ± 0.3	2.3 ± 0.5	0.6
*ps*Toc34$_{SZ}$ M79C	3.1 ± 0.4	4.2 ± 0.7	1.0
*ps*Toc34$_{SZ}$ D175C	0.8 ± 0.2	2.4 ± 0.6	0.3
*ps*Toc34$_{SZ}$ K143C	2.5 ± 0.2	1.5 ± 0.3	0.8

[a]3 μM receptor concentration.

V78C. The distribution of the FRET efficiencies is best described by two Gaussians (Figure 4B; Table 3). We observed predominant FRET efficiencies at ~95% and ~86%, which correspond to distances of 41 Å and 48 Å, respectively.

Complementary to the measured time average of FRET (taFRET) efficiencies, we determined the ensemble average of single-pair FRET (spFRET) events. The results for the GDP state were analyzed by a probability distribution analysis (PDA) (Figures 4C and S4), which shows that a single distance (43 Å) describes the data. PDA takes into consideration the fact that stochastically fluctuating fluorophores result in a Gaussian distribution for the fluorophore distances, but not for the FRET efficiencies. The deviations from a Gaussian are most significant at high FRET efficiencies. As PDA currently cannot be carried out for taFRET data, we have to assume a large error in the high FRET regime. Analogously to spFRET, the closed state observed by taFRET is analyzed by a single Gaussian, which fits the data robustly, considering the uncertainty in these measurements (Table 3).

Arginine 133 Is Essential for Homodimer Formation

The substitution of arginine 133 to alanine eliminates dimer formation of Toc34 (Reddick et al., 2007). We analyzed the influence of arginine 133 on the conformation of the G domains while being linked up to a stable dimer (Figure 2A). While measuring *ps*Toc34$_{SZ}$ V78C/R133A, we observed significantly different FRET behavior (Figure 5A) compared to *ps*Toc34$_{SZ}$ V78C (Figure 4A), with dynamics between the open and closed states on the time scale of seconds. Two populations in addition to the state described for *ps*Toc34$_{SZ}$ V78C were observed, with FRET efficiencies of 62%/60 Å and 36%/75 Å, respectively (Figure 5B; Table 3). We hold that the latter populations represent detached G domains held together by the leucine zipper, arguing that the β sheets carrying the labels would otherwise have to detach entirely from the structure to allow such large distances.

Further, we compared the binding rates of (2′,3′)-*O*-(*N*-methylanthraniloyl) (mant)-labeled GMPPNP (mant-GMPPNP) (Wilden et al., 2006) to GDP-loaded monomeric *ps*Toc34$_{\Delta TM}$ V78C, dimeric *ps*Toc34$_{SZ}$ V78C, and *ps*Toc34$_{SZ}$ V78C/R133A, noting that dimerization of Toc34 reduces the nucleotide exchange rate (Oreb et al., 2011). Receptor concentrations of 5 μM and 100 μM were used, which represent concentrations well below and above the K_D = 50 μM for homodimerization, respectively (Koenig et al., 2008). The observed association rates for binding of mant-GMPPNP to 5 μM receptor are 2.0 ± 0.1 nM/s for *ps*Toc34 V/C, 1.0 ± 0.3 nM/s for *ps*Toc34$_{EC}$ V78C/R133A,

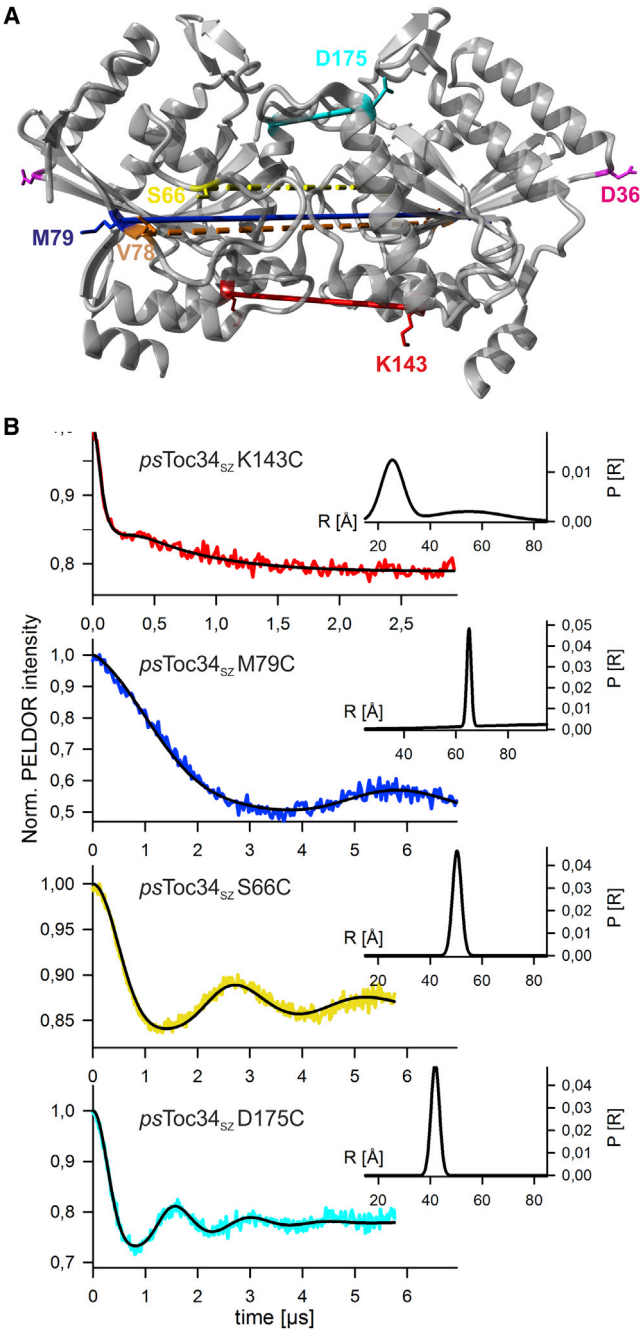

Figure 3. Assessment of the Toc34 Homodimer by PELDOR and FRET

(A) Side view of the dimeric G domains of *ps*Toc34 indicating the positions of the cysteines introduced for PELDOR and FRET.

(B) The PELDOR time traces *ps*Toc34$_{SZ}$ K143C (background-corrected; red curve), *ps*Toc34$_{SZ}$ M79C (background corrected; blue curve), *ps*Toc34$_{SZ}$ S66C (background corrected; yellow curve), and *ps*Toc34$_{SZ}$ D175C (background corrected; cyan curve) are shown. Fits (lines without noise) were obtained from one-Gaussian model fitting (*ps*Toc34$_{SZ}$ S66C and D175C) or two-Gaussian model fitting (*ps*Toc34$_{SZ}$ K143C and M79C). Obtained distance distributions are shown as insets.

See also Figure S3.

Table 2. Distance Determination by PELDOR

Protein	Nucleotide	Distance Predicted[a] (Å)	PELDOR (Å) (%)[b] Distance I	Distance II
*ps*Toc34$_{SZ}$ S66C	GDP	44	50 ± 2	none
	GMP-PNP		100 ± 48	none
	GDP-AlF$_x$		50 ± 3	none
*ps*Toc34$_{SZ}$ S66C + B1	GDP	44	48 ± 5 (50)	51 ± 2 (50)
	GMP-PNP		100 ± 42	none
	GDP-AlF$_x$		48 ± 3 (35)	50 ± 1 (65)
*ps*Toc34$_{SZ}$ M79C	GDP	64	65 ± 1 (50)	100 ± 49 (50)
	GMP-PNP		87 ± 50	none
	GDP-AlF$_x$		65 ± 4 (55)	100 ± 50 (45)
*ps*Toc34$_{SZ}$ M79C + B1	GDP	64	65 ± 2 (49)	96 ± 50 (51)
	GMP-PNP		96 ± 50	none
	GDP-AlF$_x$		66 ± 4 (59)	100 ± 50 (41)
*ps*Toc34$_{SZ}$ K143C	GDP	27	26 ± 6 (64)	55 ± 20 (36)
	GMP-PNP		49 ± 34	none
	GDP-AlF$_x$		26 ± 7 (71)	56 ± 15 (29)
*ps*Toc34$_{SZ}$ K143C + B1	GDP	27	25 ± 6 (39)	55 ± 23 (61)
	GMP-PNP		47 ± 33	none
	GDP-AlF$_x$		26 ± 7 (65)	54 ± 15 (35)
*ps*Toc34$_{SZ}$ D175C	GDP	40	42 ± 2	none
	GMP-PNP		78 ± 5	none
	GDP-AlF$_x$		42 ± 3	none
*ps*Toc34$_{SZ}$ D175C + B1	GDP	40	42 ± 3 (76)	54 ± 50 (26)
	GMP-PNP		99 ± 50	none
	GDP-AlF$_x$		42 ± 3 (72)	70 ± 30 (28)

[a]From rotamer library simulations.
[b]Data listed are distance as mean ± SD and percentage of molecules representing this population.

Table 3. Distance Determination by FRET

Protein	Nucleotide	taFRET Å[a]	taFRET FE (%)[b]	spFRET Å (%)[c]
*ps*Toc34$_{SZ}$ (WT)[d]		46	89	–
*ps*Toc34$_{SZ}$ D36C[e]		>1,00	0	–
*ps*Toc34$_{SZ}$ V78C[f]	GDP	41	95 (41)	43 (100)
		48	86.4	
		43[g]	92[g]	
	GMP-PNP	45	90 (81)	43 (66)
		60	62	55
	GDP-AlF$_x$	45	90 (91)	43 (77)
		69	42	64
*ps*Toc34$_{SZ}$ V78C[f] + B1	GDP	45	90 (45)	43 (55)
		56	72	54
	GMP-PNP	47	88 (54)	43 (51)
		60	62	52
	GDP-AlF$_x$	45	90 (50)	43 (63)
		63	55	62
*ps*Toc34$_{SZ}$ V78C/R133A[g]	GDP	43	92 (59)	ND
		60	62 (10)	
		75	36 (31)	

ND, no data; taFRET, time-average single-molecule FRET of single event; spFRET, single-pair FRET.
[a]Distance calculated from FRET efficiency.
[b]Measured FRET efficiency (FE) and percentage of population estimated from Gaussian analysis.
[c]Distance and percentage of population determined by probability distribution.
[d]The distance of the cysteines is 21 Å leading to a predicted FE (PEF) of 99.9%.
[e]The distance is 88 Å leading to a PFE of 14%
[f]The distance is 50 Å leading to a PFE of 82%.
[g]For a single Gaussian fit in analogy to spFRET.

and 0.2 ± 0.1 nM/s for *ps*Toc34$_{EC}$ V78C (Figure 5C). At a protein concentration of 100 μM, binding of mant-GMPPNP to *ps*Toc34$_{EC}$ V78C/R133A and *ps*Toc34$_{\Delta TM}$ V78C is comparable, whereas binding to *ps*Toc34$_{SZ}$ V78C is slower (Figure 5D). However, the GMPPNP binding rates of the three proteins are more comparable at high than at low protein concentrations, which is consistent with the higher fraction of *ps*Toc34$_{\Delta TM}$ V78C homodimers at higher protein concentrations and underlines the importance of arginine 133 for dimer formation.

The Nucleotide Loading State Affects the Conformation of the Toc34 Homodimer

Next, we explored the nucleotide dependence of the conformational freedom of homodimeric Toc34. To this end, *ps*Toc34$_{SZ}$ K143C, *ps*Toc34$_{SZ}$ M79C, *ps*Toc34$_{SZ}$ S66C, and *ps*Toc34$_{SZ}$ D175C (Figure 2A) were loaded with either GMPPNP or GDP and aluminum fluoride (GDP-AlF$_x$), respectively, with the latter mimicking the transition state of GTP hydrolysis (Gasper et al., 2009). For all investigated protein variants, we noted that the GDP-AlF$_x$-loaded state shows PELDOR signals similar to those observed for the GDP-loaded state (Figure S6). Detailed analysis of the traces revealed that a similar distance distribution was observed between GDP and GDP-AlF$_x$ states (Figures 6 and S6; Table 2). For the GMPPNP-loaded proteins, the PELDOR analysis yielded broad distance distributions with a dramatic increase in the frequency of larger distances (Figure S6). This observation most likely reflects a high conformational flexibility of *ps*Toc34$_{SZ}$ in the GTP state, suggesting that the γ-phosphate of GMPPNP induces intramolecular changes favoring an open conformation.

In taFRET and spFRET experiments (Figures 7 and S7) on GDP-AlF$_x$- or GMPPNP-loaded *ps*Toc34$_{SZ}$ V78C, we observed an additional open conformation for both nucleotide states (69 Å and 60 Å) (Table 3), which have not been found for the GDP-loaded receptor. However, the more opened state is more highly populated in the GMPPNP than the GDP-AlF$_x$ state, which is consistent with the PELDOR experiments. The somewhat contrasting observations for *ps*Toc34$_{SZ}$ V78C and *ps*Toc34$_{SZ}$ M79C in the GDP-AlF$_x$-loaded protein can be attributed to technical limitations. The positions of the labels in the latter variant are at a distance at which the sensitivity of PELDOR to medium-range conformational changes is significantly reduced. Taken together, the results obtained with the different techniques applied suggest that the nucleotide-loading state influences the equilibrium between different conformations of the Toc34 homodimer.

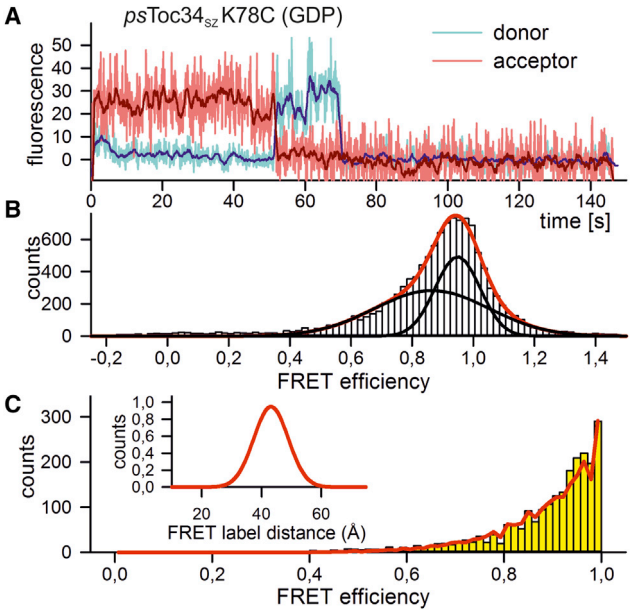

Figure 4. Assessment of the Toc34 Homodimer by FRET

(A) A representative example of the donor trace (cyan) and acceptor trace (red) of single-molecule FRET sampling for *ps*Toc34$_{SZ}$ V78C is shown.

(B) The statistical analysis of the FRET efficiency for *ps*Toc34$_{SZ}$ V78C is shown. Lines represent the least squares fit analysis to two-Gaussian model fitting (either individual results [black] or sum of all results [red]).

(C) PDA of the single-pair FRET measurement is shown for psToc34$_{SZ}$ V78C. See also Figure S4.

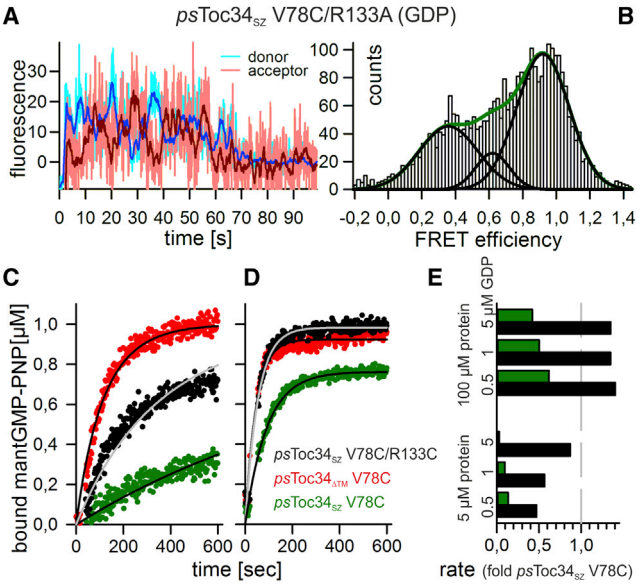

Figure 5. The Importance of Arginine 133 for the Toc34 Homodimer

(A) An example of FRET sampling for *ps*Toc34$_{SZ}$ V78C/R133A is shown, as in Figure 4A.

(B) The statistical analysis of the FRET efficiency for *ps*Toc34$_{SZ}$ V78C/R133A is shown, as in Figure 3B.

(C and D) The association of mant-GMPPNP with *ps*Toc34$_{\Delta TM}$ V78C (red), *ps*Toc34$_{SZ}$ V78C (green), and *ps*Toc34$_{SZ}$ V78C/R133A (black) was determined by fluorescence anisotropy measurements and subsequently normalized to bound mant-GMPPNP. The time-dependent binding of 1 µM mant-GMPPNP to (C) 5 µM or (D) 100 µM protein is shown. Lines indicate the least squares fit analysis as outlined in the Supplemental Information.

(E) The ratio of the binding rate constants determined for *ps*Toc34$_{SZ}$ V78C (green) or *ps*Toc34$_{SZ}$ V78C/R133A (black) and *ps*Toc34$_{\Delta TM}$ V78C at indicated concentrations is shown.

The Transit Peptide Affects the Dimer in a Nucleotide-Dependent Manner

Toc34 has been considered as a receptor for preproteins (Schleiff and Becker, 2011). We analyzed the influence of a 28–aa-long peptide comprising the C terminus of the transit peptide of the small subunit of ribulose 1,5-bisphosphate carboxylase, or RuBisCO (B1 peptide) (Becker et al., 2004), on the structure and dynamics of the homodimer. Some of the PELDOR time traces show slight changes upon addition of the peptide (Figures S5 and S6), which suggest an increase in the open dimer population for GDP-loaded *ps*Toc34$_{SZ}$ K143C and D175C, as well as for the GDP-AlF$_x$-loaded *ps*Toc34$_{SZ}$ D175C variant (Figure 6; Table 2). The PELDOR signal of the GMPPNP-loaded state is largely unaffected after addition of the peptide (Figures 6, S5, and S6; Table 2). For the aforementioned reasons, significant conformational changes cannot be concluded for *ps*Toc34$_{SZ}$ M79C in the presence of the peptide, whereas the FRET measurements for *ps*Toc34$_{SZ}$ V79C are more sensitive with respect to alterations. Consistently in single-molecule taFRET and spFRET experiments, we observed a significant increase in the population with larger distance after addition of the B1 peptide for all nucleotides, which documents that binding of peptide to the dimer induces an opening.

The observed peptide-induced dimer opening prompted a further analysis of the interaction between both. We applied fluorescence anisotropy measurements, which describe the (rotational) mobility of a fluorescent label being fused to the peptide. For free diffusing peptide, we observed an anisotropy of r = 0.06 ± 0.01 (Figure 8, top). Titration of the peptide to 10 µM Toc34 loaded with GDP or GDP-AlF$_x$ shows a more drastic increase of the anisotropy for the latter, whereas addition of peptide to the GMPPNP-loaded Toc34 homodimer revealed the same result as for the GDP-loaded receptor (Figure S8). The analyses of preprotein binding revealed a K_D of 5 µM. A twofold higher anisotropy was observed when the peptide was added to the GDP-AlF$_x$-loaded dimer. The association of peptide to the GDP-loaded *ps*Toc34$_{SZ}$ V78C is too rapid to be monitored after the stirring period. Regarding GDP-AlF$_x$-loaded *ps*Toc34$_{SZ}$ V78C, we observed an increase in both fluorescence intensities, both of which are saturated after ~200 s (Figure 8, bottom). Thus, the GDP-AlF$_x$-loaded dimer exhibits a binding behavior to the peptide that is significantly distinct from the GDP- and GMPPNP-loaded states and exhibits a clearly different binding rate.

DISCUSSION

GADs are involved in multiple essential cellular processes. Their dimerization has been considered essential for the regulation of the GTPase cycle, replacing the need for a GAP (Gasper et al., 2009). The GTPase Toc34, which is part of the TOC complex (Schleiff et al., 2003), dimerizes in vitro (Bionda et al., 2008; Koenig et al., 2008) and in the context of the TOC complex

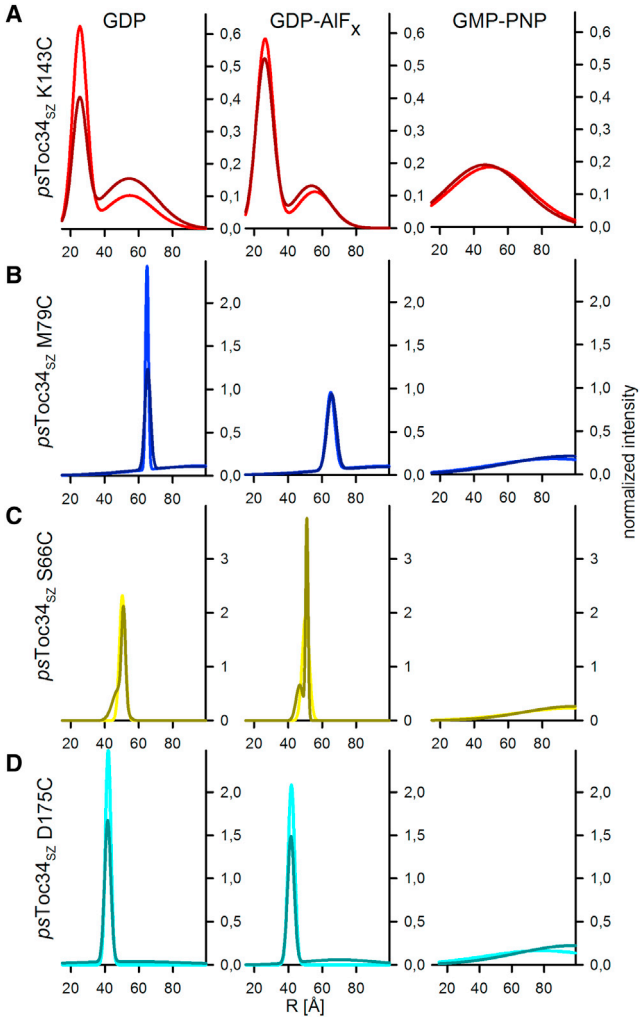

Figure 6. Influence of Nucleotides and Transit Peptides on the Homodimer of Toc34 Assayed by PELDOR

(A–D) The obtained distance distributions from background-corrected PELDOR time traces for 100 μM dimers of indicated proteins loaded with GMPPNP, GDP-AlF$_x$, or GDP (indicated at top) in the absence (bright line) or presence of 1 mM B1 peptide (dark line) are shown.

See also Figures S5 and S6.

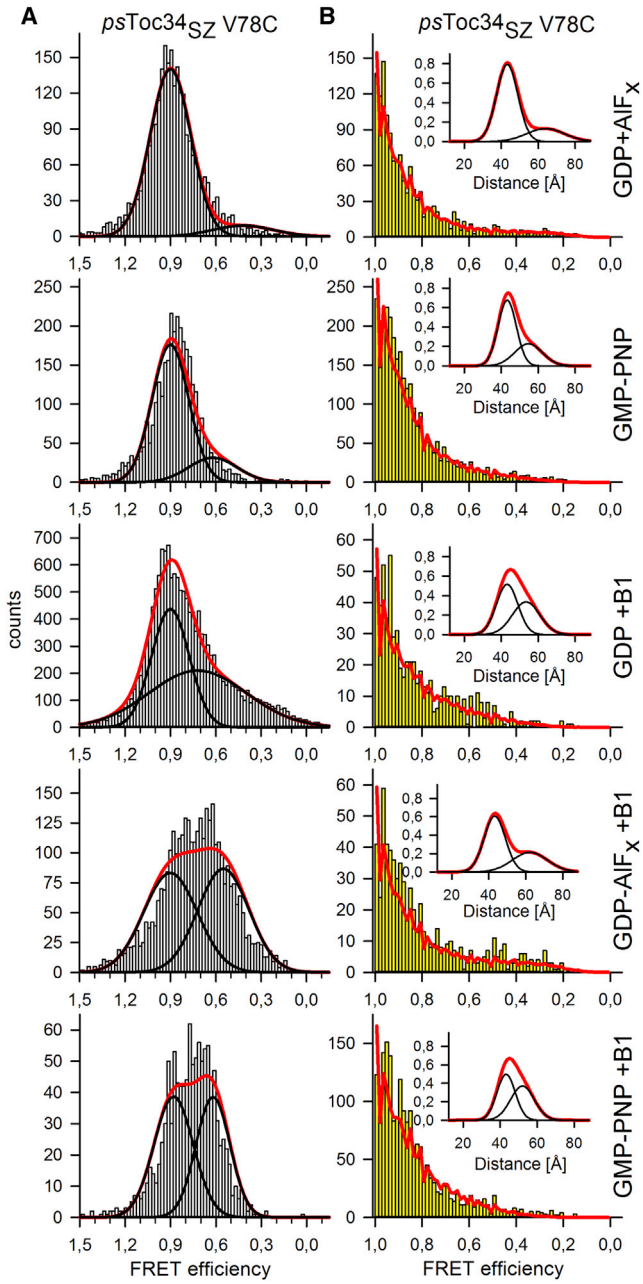

Figure 7. Toc34 FRET Is Dependent on Nucleotides and Transit Peptides

(A and B) The statistical analysis of the single-molecule taFRET efficiency recordings (A) and single-pair FRET measurements (B) of *ps*Toc34$_{EC}$ V/C loaded with the indicated nucleotides is shown. The influence of B1 peptide [1 mM (A) or 330 μM (B)] on the signal observed for the different nucleotide loading states is shown.

See also Figure S7.

(Figure 1A). Its homodimerization is thought to regulate nucleotide exchange, because the nucleotide binding site is positioned at the dimerization interface (Koenig et al., 2008; Oreb et al., 2011). In this paper, we describe structural changes in the short and long range on the basis of three complementary methods: taFRET, spFRET, and PELDOR. This combination enabled us to monitor conformational changes of the Toc34 dimer at the side of the protein that is expected to be exposed to the membrane surface (*ps*Toc34$_{SZ}$ K143C), at the side of the protein that faces the cytosol (*ps*Toc34$_{SZ}$ D175C), and within (*ps*Toc34$_{SZ}$ S66C) and opposite to the dimerization interface (*ps*Toc34$_{SZ}$ V78C, *ps*Toc34$_{SZ}$ M79C).

The GDP-loaded receptor forms a tight dimeric conformation, as judged from the close proximity of the labels (Tables 2 and 3) at positions S66C, K143C, D175C, and M79C (for PELDOR) and at position V78C (for FRET). This is consistent with the proposed inhibition of GTP/GDP exchange by dimerization (Oreb et al., 2011). The Toc34 dimer at the transition state (GDP-AlF$_x$) is in a conformation comparable to that in the GDP state, as judged from the label distances (Figure 9). The GMPPNP-loaded dimer shows a distinct and more flexible

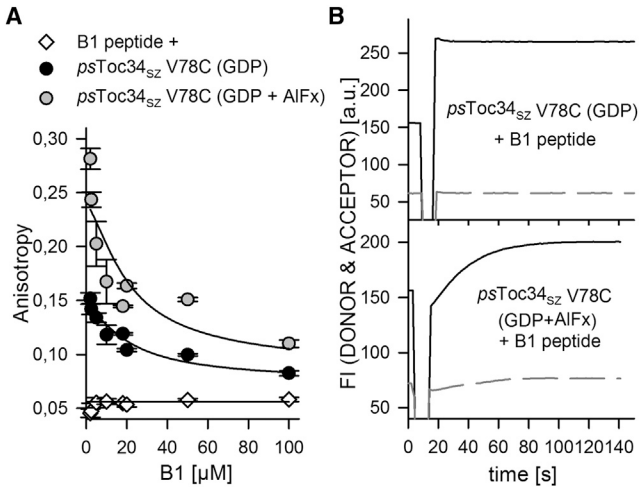

Figure 8. The Interaction of the Transit Peptide Fragment B1

(A) Anisotropy of the fluorescence-labeled B1 peptide dependent on the concentration for three different cases: the free unbound B1 peptide in the presence of GDP-loaded or GDP-AlF$_x$-loaded *ps*Toc34$_{SZ}$ V78C (10 μM).

(B) *ps*Toc34$_{SZ}$ V78C (5 μM) either loaded with GDP or GDP-AlF$_x$ was equilibrated for 30 s before 1 mM of unlabeled B1 peptide was added, followed by mixing (without fluorescence monitoring) for 15 s. The fluorescence intensities at 575 nm (black line; donor maximum) and 665 nm (dashed line; acceptor maximum) were recorded. An increase in donor signal corresponds to an opening of the dimer.

See also Figure S8.

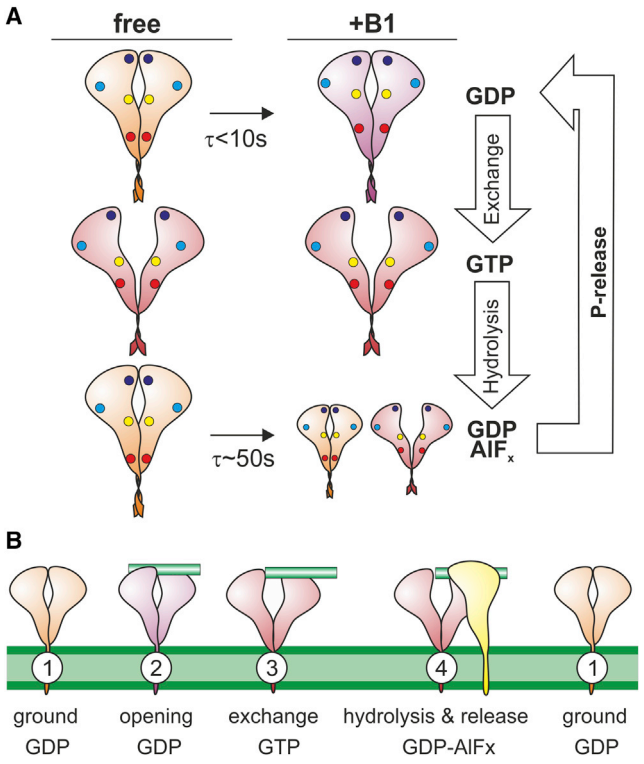

Figure 9. The Postulated Interdependency of Substrate Binding and Nucleotide-Dependent Dimerization of Toc34

(A) A model of the three states discussed in the manuscript is shown. The state with shortest distances is shown in orange (found for GDP and GDP-AlF$_x$), the state with largest distances is shown in red (found for GMPPNP), the state induced by B1 in violet (found for GDP and GDP-AlF$_x$ + B1). The positions of the labels are indicated with colored dots (blue, D175C; yellow, S66C; cyan, V78C; and red, K143C). Note that, for +B1, only the state that is more enriched is shown. For the sake of simplicity, we emphasize only the major changes between nucleotides and excluded alterations of the model representing the changes enforced by the B1 peptide.

(B) The conformations are visualized for the different molecular events during preprotein recognition and transfer as discussed in the text. The GDP-loaded state of dimeric Toc34 in the context of the TOC complex (image 1) most likely recognizes incoming preproteins (green; image 2). The induced opening of the dimer allows for nucleotide exchange (image 3), resulting in the transition to the GTP state, leading to monomerization of Toc34, which might subsequently be able to interact with downstream components of the TOC complex (e.g., Toc159, yellow; image 4), whereas GTP hydrolysis redirects the Toc34 back to the ground state. The nucleotide loading state of the receptor is indicated below. The GTP state in the absence of peptide is not considered here.

conformation, as we observed long distances with a broad distribution by PELDOR and a state with larger FRET label distance (Figures 6 and 7; Tables 2 and 3).

Addition of preprotein in terms of the B1 peptide to the GDP-loaded receptor variants (*ps*Toc34$_{SZ}$ K143C and D175C [PELDOR]) and V78C (FRET) slightly enforces a more relaxed conformation as the population of the larger distance increases with respect to the receptor in absence of B1 (Figures 6, 7, and 9; Tables 2 and 3). This more relaxed conformation does not reflect a complete disassembly of the dimer, which is seen for the R133A mutant with average distance of 75 Å (FRET) (Reddick et al., 2007) (Figures 4 and 6; Table 3). The peptide-induced opening strongly implies that dimerization of Toc34 is regulated by its substrate binding.

Remarkably, the dimeric GDP state shows very fast kinetics for the recognition of peptides (Figure 8), and the observed K_D of 5 μM for peptide binding to the dimer is one order of magnitude lower than that of the monomeric receptor (K_D = 90 μM) (Schleiff et al., 2002). This suggests that a dimeric conformation of Toc34 rather than the monomeric protein serves as a receptor for the incoming preprotein. Remarkably, the dimer at the transition state (GDP-AlF$_x$) shows a reduced binding rate and transit peptide mobility compared with the GDP- or GMPPNP-loaded state (Figures 8 and S8), whereas the presence of the transit peptide does not dramatically alter the structure. Addition of the substrate induced an increase of the population with a longer distance for *ps*Toc34$_{SZ}$ V78C, whereas *ps*Toc34$_{SZ}$ D175C showed in general a larger distance than before addition of the peptide (Figure 6; Table 3).

By transferring these findings to the native system, we could extract the following model (Figure 9): Preproteins are recognized by the Toc34 dimer via their transit peptides. The intrinsic GTPase activity of Toc34 (Jelic et al., 2002) suggests that the homodimer has a GDP-loaded ground state, which most likely recognizes incoming preproteins (Sommer and Schleiff, 2009) (Figure 8). The preprotein-induced transition of the dimer conformation (Figure 9A and 9B, 1 to 2) induces nucleotide exchange (Oreb et al., 2011) (Figure 9B, 2 to 3), which in turn results in a further opening of the homodimer, as we found for the GMPPNP state in general (Figure 9A). It has to be mentioned that we could not discriminate between rearrangement of the two monomeric

units in the dimer as found, e.g., in the MnmE GTPase cycle analyzed by electron paramagnetic resonance (EPR) spectroscopy (Böhme et al., 2010), nor could we discriminate local structural changes within each monomer as observed, e.g., for Rab8 upon GEF binding (Itzen et al., 2006). However, irrespective of the mode, the peptide-induced structural changes are a prerequisite for the nucleotide exchange.

The broad distances found for the GMPPNP state, which point to a dimer opening, are consistent with the idea that monomeric Toc34 is able to interact with downstream components of the TOC complex (Figure 9B, 3 to 4). It has been suggested that GTP-loaded monomeric Toc34 possesses enhanced affinity for Toc159 in the presence of preprotein (Becker et al., 2004). However, whether GTP hydrolysis is the trigger for subsequent preprotein transfer or whether the observed state is reminiscent of the Toc159-Toc34 heterodimer cannot be distinguished at this stage. Nevertheless, considering the increase of the dissociation constant for B1 by one order of magnitude and the very slow rate of the transition state (Figure 8), we are confident that B1 is released from monomeric GTP-loaded Toc34. Accordingly, GTP hydrolysis would trigger homodimerization of the substrate-free receptor, and, indeed, the C-proximal part of the protein (monitored in *ps*Toc34$_{SZ}$ K143C by PELDOR) shows a significant increase in the more open population when GMPPNP and GDP-AlF$_x$ states are compared (Figure 6A). The central region (inspected by FRET) does not show an alteration of the population (Figure 9B, image 3, "exchange GTP"). Completion of hydrolysis finalizes the reaction cycle by stabilizing the association of the central region as well (Figure 9B, 4 to 1).

In sum, we suggest that the regulatory function of Toc34 is transmitted by substrate binding, in contrast to bona fide G proteins, with conformational changes in direct response to their nucleotide-loading state (Gasper et al., 2010). Accordingly, the equilibrium between conformational states 1 and 2 (Figure 9B) is interpreted as inherent flexibility of the GTP-binding motives in response to GTP's γ-phosphate, as shown for other G proteins of the TRAFAC class, such as p21 Ras (Halkides et al., 1994). Structural analyses by nuclear magnetic resonance or EPR spectroscopy generally posit a more dynamic nature for the switch regions, e.g., the ability of Ras proteins to occupy two different conformations in the GTP-bound state (Wittinghofer and Vetter, 2011). Interestingly, elongation factor G (EF-G), a TRAFAC GTPase, shows no structural changes in the switch regions in the GTP- and GDP-bound states (Hansson et al., 2005) unless it is bound to the ribosome (Gao et al., 2009; Stark et al., 2000), indicating that its presence is required for the nucleotide-dependent switch of EF-G (Wittinghofer and Vetter, 2011). Thus, the structural dynamics of bona fide G proteins induced by GTP hydrolysis are replaced by substrate-dependent dimer flexibility, which might constitute a general regulatory mode. This concept might even hold true for members of the SIMIBI superfamily. The cytoplasmic GTPase Xab1 is dimeric, regardless of the bound nucleotide, and only small structural changes take place when the nucleotide is exchanged (Gras et al., 2007). Xab1 might be regulated by a mechanism that is similar to that of the Toc34 homodimer, which is different from the dimerization-dependent switch mechanism known from SRP/SR (Gras et al., 2007). In turn, the dimerization-dependent switch mechanism known from SRP/SR might be relevant for the regulation of the Toc34/Toc159 heterodimer. Accordingly, within the TOC reaction cycle, the regulatory mode described herein and the dimerization-dependent switch mechanism might act in concert.

EXPERIMENTAL PROCEDURES

General Methods

The peptide B1 (MVAPFTGLKSAAS(PO3)-PVSRKQNLDITSC) (Becker et al., 2004), multiple turnover measurements, and size exclusion analysis have been described previously (Oreb et al., 2011). mRNAs coding full-length *ps*Toc34 (*ps*Toc34$_{FL}$) and its variants were synthesized by in vitro transcription using linearized DNA and SP6 RNA polymerase. Chloroplasts were isolated from 7- to 8-day-old *Pisum sativum*, and import was performed as described by Becker et al. (2004). For crosslinking, samples were irradiated from above (~10 cm) with 254-nm UV light bulbs (Stratalinker UV Crosslinker 2400; Stratagene) for 20 min. High-definition native-PAGE and corresponding sample preparation were carried out as described by Ladig et al. (2011). For detailed information, see the Supplemental Information.

Construct Generation

*ps*Toc34$_{FL}$ was amplified from cDNA and cloned into pSP65. *ps*Toc34$_Z$ was generated by inserting the neck coiled-coil from kinesin-1 (Bornschlögl et al., 2009) between the C-terminal His-tag and the G domain of Toc34, which was amplified by PCR and cloned via XhoI/SalI into XhoI-linearized *ps*Toc34$_{\Delta TM}$ (Schleiff et al., 2002). To enhance the degrees of freedom, a non-coiled-coil-forming spacer segment was amplified and inserted into *ps*Toc34$_Z$ between the G domain and the coiled-coil sequence (*ps*Toc34$_{SZ}$). Point mutations were inserted using the QuikChange Site-Directed Mutagenesis Kit protocol (Stratagene). The primers used are listed in Table S1.

Recombinant Production and Purification of Proteins

All proteins and protein variants were recombinantly expressed in *Escherichia coli* BL21. Cells were grown in lysogeny broth supplemented with 10 μg/ml ampicillin at 37°C to a 600-nm wavelength optical density of 0.8. Protein expression was induced for 3.5 hr at 37°C by addition of 1 mM isopropyl β-D-1-thiogalactopyranoside (final). Cells were harvested by centrifugation at 5,000 × g for 5 min at room temperature and lysed for 30 min on ice in 20 mM Tris-HCl, pH 8, 300 mM NaCl, 5 mM MgCl2, 10% (v/v) glycerol with 1 mM phenylmethanesulfonyl fluoride, 5 μg/ml DNaseI and 2 mg/ml lysozyme. Cells were sonified, and cell debris was precipitated by centrifugation (30 min at 25,000 × g at 4°C). Soluble proteins were bound to a Ni-nitrilotriacetic acid agarose column (QIAGEN), washed (5× 10 bed volumes) with 20 mM Tris-HCl, pH 8, 300 mM NaCl, 15 mM imidazole, 5 mM $MgCl_2$, and 10% (v/v) glycerol, then eluted with 5× bed volumes of 20 mM Tris-HCl, pH 8, 300 mM NaCl, 400 mM imidazole, 5 mM $MgCl_2$, and 10% (v/v) glycerol.

For nucleotide exchange or site-directed spin-labeling using 1-oxyl-2,2,5,5-tetramethylpyrroline-3-methyl)methanethiosulfonate (MTSSL) (Enzo Life Sciences), matrix-bound protein was incubated overnight with 1× bed volume of lysis buffer supplemented with 1 mM concentrations of GDP, GTP (GMPPNP), and GDPAlF$_x$ and/or 2 mg of MTSSL (in MeOH); washed; and eluted. Proteins were further purified by size exclusion chromatography using a Superdex 200 10/300 column (GE Healthcare Life Sciences) in 20 mM Tris-HCl, pH 7, 300 mM NaCl, 5 mM $MgCl_2$, and 10% (v/v) glycerol. Fractions were collected and concentrated using Amicon® Ultra-15, 30 kDa MWCO centrifugal filter units (EMD Millipore). Buffer exchange (25 mM 2-[4-(2-hydroxyethyl) piperazin-1-yl]ethanesulfonic acid /NaOH, pH 8, 300 mM NaCl, 5 mM $MgCl_2$, and 30% (v/v) glycerol) was performed in the same microcentrifuge concentrator.

PELDOR Measurements

All samples (5–10 μl at 160–200 μM concentration) were transferred to EPR tubes with a 1.6 mm outer diameter. The samples were shock-frozen in liquid nitrogen. Pulsed EPR data were measured on an ELEXSYS E580 EPR spectrometer (Bruker) equipped with a Bruker PELDOR unit (E580-400U), a continuous flow helium cryostat (CF935; Oxford Instruments), and a temperature control system (ITC 502; Oxford Instruments). For the *ps*Toc34$_{SZ}$

variants, the PELDOR experiments were carried out at Q-band frequencies (33.7 GHz) with the ELEXSYS SuperQ-FT accessory unit and a Bruker AmpQ 10 W amplifier. The cavity is a Bruker EN5107D2. A custom-made pulse-shaping unit was implemented and utilized for the measurements of M79C, S66C, and D175C variants as described elsewhere (Spindler et al., 2012). The temperature was kept at 50 K. The shot repetition time was 4–5 ms.

For PELDOR experiments, the dead-time free four-pulse sequence was used (Pannier et al., 2000). The pulse length was 32 ns ($\pi/2$ and π) for probe pulses, with a 20-ns (π) pump pulse used for the psToc34$_{SZ}$ K143C variant and an 80 (50) MHz sech/tanh adiabatic pump pulse with a length of 360 (400) ns (Spindler et al., 2013) used for the psToc34SZ M79C (S66C and D175C) variants, respectively. The pulse separation between the second and third probe pulses was between 2.6 and 8.5 μs, depending on the probed distances and the transversal relaxation time (T_m) of the samples. The pump pulse was placed on the maximum of the nitroxide absorption spectrum, and the probe frequency was chosen 70 MHz lower.

PELDOR data were processed using the DeerAnalysis2013 software package (Jeschke et al., 2006), with corrections made for background decay using a homogeneous 3D spin distribution. Tikhonov regularization was performed with a regularization parameter (α) of 1,000 chosen according to the L-curve criteria. The final distance distributions were obtained by fitting the experimental time domain data to a model that assumes a distance distribution consisting of one or two Gaussians.

In silico spin labeling of the *ps*Toc34 structure (Protein Data Bank ID 3BB1; Koenig et al., 2008) using the rotamer library approach and estimation of inter-spin distances were performed with the MMM 2013 software package (Polyhach et al., 2011).

Fluorescence Measurements

ATTO 550 and ATTO 647N (ATTO-TEC GmbH) were covalently attached to cysteine at a ratio of 1:1 (fluorophore:protein). Peptide was labeled at an engineered C-terminal cysteine with Atto550 at a ratio of 1:10 (fluorophore:peptide) to avoid detector saturation.

taFRET

taFRET measurements were carried out in a custom-built, objective-type total internal reflection fluorescence microscope. Fluorescently labeled molecules were tethered to a biotin-polyethylene glycol-coated coverslip. This functionalized coverslip is part of a microfluidic chamber mounted in a custom-built, objective-type TIRF microscope. Labeled molecules were excited by lasers at 532 nm (Compass 215M, 75 mW; Coherent) or at 635 nm (Lasiris 50 mW laser; StockerYale) through a high numerical aperture (NA) objective (NA = 1.49; Nikon Instruments) in TIRF geometry. Fluorescent light was detected through the same lens objective and separated into donor and acceptor fluorescence while being recorded by an iXon DV887 camera (Andor Technology). Movies were analyzed with a program based on IGOR Pro (WaveMetrics). Time traces of single fluorophores were extracted from the movie with a threshold criterion. The two colors were overlaid, and the corrected FRET efficiency and distances were calculated (see Supplemental Information). FRET efficiencies (every single data point) were cumulated into a histogram. Distances between the fluorophores fluctuate stochastically and are therefore expected to have a Gaussian distribution. Initial approximation indicates that this results in Gaussian distributions for the FRET efficiency of a single state (exactly: a β function).

spFRET

FRET efficiencies of free diffusing TOC dimers were measured in a home-built confocal microscope with previously published setups (Müller et al., 2005). Time traces of photon intensities were measured with (1) two single-photon avalanche photodiodes (PDM-50 μm; PicoQuant) for green and red light detection and (2) a data acquisition system (HydraHarp 400; PicoQuant). Two pulsed diode lasers (532 nm LDH-P-FA-530 and 640 nm LDH-D-C-640; PicoQuant) served as excitation sources and an apochromatic 60× water immersion lens objective (Nikon Instruments) was used. Single-molecule bursts were identified using an all-photon burst search to look for at least 10 photons within 500 ms and requiring a total of 50 photons (Nir et al., 2006). For each burst, stoichiometry and FRET efficiency values were calculated and correlated in a 2D plot to separate true FRET events from donor-only and acceptor-only events. FRET efficiency histograms were corrected for efficiencies of the detectors, quantum efficiencies of the dyes, and crosstalk caused by leakage of donor fluorescence in the red channel. To separate structural heterogeneities of the TOC dimers from stochastic variations, probability distribution analysis was performed (Antonik et al., 2006).

Fluorescence Quantification

Single-Molecule taFRET

FRET efficiencies are calculated by Equation 1,

$$E = \frac{I_{AD}}{\gamma \times I_{DA} + I_{AD}} \qquad \text{(Equation 1)}$$

where I_{AD} is the fluorescence intensity of the acceptor fluorophore (in presence of donor) and I_{DA} is the fluorescence intensity of the donor fluorophore (in presence of acceptor). The factor γ corrects for the different quantum efficiencies of the two dyes and for the detection efficiencies in the two detector channels. FRET distances are calculated by Equation 2,

$$d = R_0 \sqrt[6]{\frac{1-E}{E}} \qquad \text{(Equation 2)}$$

where R_0 is the Förster distance, and E is the measured FRET efficiency.

Fluorescence anisotropy

mant-GppNHp or mant-GMPPNP (Jena Bioscience GmbH) or labeled transit peptide was excited with vertical linear polarized light, then the vertical ($I_{\parallel}$) and horizontal ($I_{\perp}$) components of the detection were measured. Anisotropy was calculated by Equation 3 with the instrument factor G, which takes into account the different sensitivity of the detector for the two polarizations.

$$r = \frac{I_{\parallel} - G I_{\perp}}{I_{\parallel} + 2G I_{\perp}} \qquad \text{(Equation 3)}$$

Statistics

Data are presented as mean ± SD. Statistical significance was assessed using SigmaPlot version 12 software (Systat Software).

SUPPLEMENTAL INFORMATION

Supplemental Information includes Supplemental Experimental Procedures, eight figures, one table, and Supplemental References and can be found with this article online at http://dx.doi.org/10.1016/j.str.2014.02.004.

ACKNOWLEDGMENTS

We thank Matthias Rief (Technical University Munich) for providing the templates for the *dm*KHC coiled-coil. This study was supported by the Deutsche Forschungsgemeinschaft (SFB-807 and CEF to E.S. and T.F.P. and NIM to T.H.), the Volkswagenstiftung (to E.S.), the CMP Frankfurt (to E.S.), the IMPRESS of the MPI of Biophysics (to K.W.), and the CompInt program of the Elitenetzwerk Bayern (to C.L.).

Received: September 19, 2013
Revised: January 29, 2014
Accepted: February 1, 2014
Published: March 13, 2014

REFERENCES

Antonik, M., Felekyan, S., Gaiduk, A., and Seidel, C.A. (2006). Separating structural heterogeneities from stochastic variations in fluorescence resonance energy transfer distributions via photon distribution analysis. J. Phys. Chem. B *110*, 6970–6978.

Aronsson, H., Combe, J., Patel, R., Agne, B., Martin, M., Kessler, F., and Jarvis, P. (2010). Nucleotide binding and dimerization at the chloroplast preprotein import receptor, atToc33, are not essential in vivo but do increase import efficiency. Plant J. *63*, 297–311.

Bauer, J., Hiltbrunner, A., Weibel, P., Vidi, P.A., Alvarez-Huerta, M., Smith, M.D., Schnell, D.J., and Kessler, F. (2002). Essential role of the G-domain in

targeting of the protein import receptor atToc159 to the chloroplast outer membrane. J. Cell Biol. *159*, 845–854.

Becker, T., Jelic, M., Vojta, A., Radunz, A., Soll, J., and Schleiff, E. (2004). Preprotein recognition by the Toc complex. EMBO J. *23*, 520–530.

Bian, X., Klemm, R.W., Liu, T.Y., Zhang, M., Sun, S., Sui, X.W., Liu, X.Q., Rapoport, T.A., and Hu, J.J. (2011). Structures of the atlastin GTPase provide insight into homotypic fusion of endoplasmic reticulum membranes. Proc. Natl. Acad. Sci. USA *108*, 3976–3981.

Bionda, T., Koenig, P., Oreb, M., Tews, I., and Schleiff, E. (2008). pH sensitivity of the GTPase Toc33 as a regulatory circuit for protein translocation into chloroplasts. Plant Cell Physiol. *49*, 1917–1921.

Böhme, S., Meyer, S., Krüger, A., Steinhoff, H.J., Wittinghofer, A., and Klare, J.P. (2010). Stabilization of G domain conformations in the tRNA-modifying MnmE-GidA complex observed with double electron electron resonance spectroscopy. J. Biol. Chem. *285*, 16991–17000.

Bornschlögl, T., Woehlke, G., and Rief, M. (2009). Single molecule mechanics of the kinesin neck. Proc. Natl. Acad. Sci. USA *106*, 6992–6997.

Bos, J.L., Rehmann, H., and Wittinghofer, A. (2007). GEFs and GAPs: critical elements in the control of small G proteins. Cell *129*, 865–877.

Chappie, J.S., Acharya, S., Leonard, M., Schmid, S.L., and Dyda, F. (2010). G domain dimerization controls dynamin's assembly-stimulated GTPase activity. Nature *465*, 435–440.

DerMardirossian, C., and Bokoch, G.M. (2005). GDIs: central regulatory molecules in Rho GTPase activation. Trends Cell Biol. *15*, 356–363.

Focia, P.J., Shepotinovskaya, I.V., Seidler, J.A., and Freymann, D.M. (2004). Heterodimeric GTPase core of the SRP targeting complex. Science *303*, 373–377.

Ford, M.G.J., Jenni, S., and Nunnari, J. (2011). The crystal structure of dynamin. Nature *477*, 561–566.

Gao, Y.G., Selmer, M., Dunham, C.M., Weixlbaumer, A., Kelley, A.C., and Ramakrishnan, V. (2009). The structure of the ribosome with elongation factor G trapped in the posttranslocational state. Science *326*, 694–699.

Gasper, R., Meyer, S., Gotthardt, K., Sirajuddin, M., and Wittinghofer, A. (2009). It takes two to tango: regulation of G proteins by dimerization. Nat. Rev. Mol. Cell Biol. *10*, 423–429.

Gasper, R., Sot, B., and Wittinghofer, A. (2010). GTPase activity of Di-Ras proteins is stimulated by Rap1GAP proteins. Small GTPases *1*, 133–141.

Gras, S., Chaumont, V., Fernandez, B., Carpentier, P., Charrier-Savournin, F., Schmitt, S., Pineau, C., Flament, D., Hecker, A., Forterre, P., et al. (2007). Structural insights into a new homodimeric self-activated GTPase family. EMBO Rep. *8*, 569–575.

Halkides, C.J., Farrar, C.T., Larsen, R.G., Redfield, A.G., and Singel, D.J. (1994). Characterization of the active site of p21 ras by electron spin-echo envelope modulation spectroscopy with selective labeling: comparisons between GDP and GTP forms. Biochemistry *33*, 4019–4035.

Hansson, S., Singh, R., Gudkov, A.T., Liljas, A., and Logan, D.T. (2005). Crystal structure of a mutant elongation factor G trapped with a GTP analogue. FEBS Lett. *579*, 4492–4497.

Hwang, I., and Robinson, D.G. (2009). Transport vesicle formation in plant cells. Curr. Opin. Plant Biol. *12*, 660–669.

Itzen, A., Pylypenko, O., Goody, R.S., Alexandrov, K., and Rak, A. (2006). Nucleotide exchange via local protein unfolding—structure of Rab8 in complex with MSS4. EMBO J. *25*, 1445–1455.

Jelic, M., Sveshnikova, N., Motzkus, M., Hörth, P., Soll, J., and Schleiff, E. (2002). The chloroplast import receptor Toc34 functions as preprotein-regulated GTPase. Biol. Chem. *383*, 1875–1883.

Jeschke, G., Chechik, V., Ionita, P., Godt, A., Zimmermann, H., Banham, J., Timmel, C.R., Hilger, D., and Jung, H. (2006). DeerAnalysis2006—a comprehensive software package for analyzing pulsed ELDOR data. Appl. Magn. Reson. *30*, 473–498.

Kikuchi, S., Hirohashi, T., and Nakai, M. (2006). Characterization of the preprotein translocon at the outer envelope membrane of chloroplasts by blue native PAGE. Plant Cell Physiol. *47*, 363–371.

Koenig, P., Oreb, M., Höfle, A., Kaltofen, S., Rippe, K., Sinning, I., Schleiff, E., and Tews, I. (2008). The GTPase cycle of the chloroplast import receptors Toc33/Toc34: implications from monomeric and dimeric structures. Structure *16*, 585–596.

Ladig, R., Sommer, M.S., Hahn, A., Leisegang, M.S., Papasotiriou, D.G., Ibrahim, M., Elkehal, R., Karas, M., Zickermann, V., Gutensohn, M., et al. (2011). A high-definition native polyacrylamide gel electrophoresis system for the analysis of membrane complexes. Plant J. *67*, 181–194.

Lee, J.H., Wang, F., and Schnell, D.J. (2009). Toc receptor dimerization participates in the initiation of membrane translocation during protein import into chloroplasts. J. Biol. Chem. *284*, 31130–31141.

Leipe, D.D., Wolf, Y.I., Koonin, E.V., and Aravind, L. (2002). Classification and evolution of P-loop GTPases and related ATPases. J. Mol. Biol. *317*, 41–72.

Ling, Q.H., Huang, W.H., Baldwin, A., and Jarvis, P. (2012). Chloroplast biogenesis is regulated by direct action of the ubiquitin-proteasome system. Science *338*, 655–659.

Meyer, S., Böhme, S., Krüger, A., Steinhoff, H.J., Klare, J.P., and Wittinghofer, A. (2009). Kissing G domains of MnmE monitored by X-ray crystallography and pulse electron paramagnetic resonance spectroscopy. PLoS Biol. *7*, e1000212.

Milov, A.D., Ponomarev, A.B., and Tsvetkov, Y.D. (1984). Electron-electron double resonance in electron spin echo: model biradical systems and the sensitized photolysis of decalin. Chem. Phys. Lett. *110*, 67–72.

Müller, B.K., Zaychikov, E., Bräuchle, C., and Lamb, D.C. (2005). Pulsed interleaved excitation. Biophys. J. *89*, 3508–3522.

Nir, E., Michalet, X., Hamadani, K.M., Laurence, T.A., Neuhauser, D., Kovchegov, Y., and Weiss, S. (2006). Shot-noise limited single-molecule FRET histograms: comparison between theory and experiments. J. Phys. Chem. B *110*, 22103–22124.

Nitta, M., Saijo, M., Kodo, N., Matsuda, T., Nakatsu, Y., Tamai, H., and Tanaka, K. (2000). A novel cytoplasmic GTPase XAB1 interacts with DNA repair protein XPA. Nucleic Acids Res. *28*, 4212–4218.

Oh, Y., and Bi, E. (2011). Septin structure and function in yeast and beyond. Trends Cell Biol. *21*, 141–148.

Oreb, M., Höfle, A., Koenig, P., Sommer, M.S., Sinning, I., Wang, F., Tews, I., Schnell, D.J., and Schleiff, E. (2011). Substrate binding disrupts dimerization and induces nucleotide exchange of the chloroplast GTPase Toc33. Biochem. J. *436*, 313–319.

Pannier, M., Veit, S., Godt, A., Jeschke, G., and Spiess, H.W. (2000). Dead-time free measurement of dipole-dipole interactions between electron spins. J. Magn. Reson. *142*, 331–340.

Polyhach, Y., Bordignon, E., and Jeschke, G. (2011). Rotamer libraries of spin labelled cysteines for protein studies. Phys. Chem. Chem. Phys. *13*, 2356–2366.

Ratzke, C., Berkemeier, F., and Hugel, T. (2012). Heat shock protein 90's mechanochemical cycle is dominated by thermal fluctuations. Proc. Natl. Acad. Sci. USA *109*, 161–166.

Reddick, L.E., Vaughn, M.D., Wright, S.J., Campbell, I.M., and Bruce, B.D. (2007). In vitro comparative kinetic analysis of the chloroplast Toc GTPases. J. Biol. Chem. *282*, 11410–11426.

Roy, R., Hohng, S., and Ha, T. (2008). A practical guide to single-molecule FRET. Nat. Methods *5*, 507–516.

Scheffzek, K., Ahmadian, M.R., and Wittinghofer, A. (1998). GTPase-activating proteins: helping hands to complement an active site. Trends Biochem. Sci. *23*, 257–262.

Schiemann, O., and Prisner, T.F. (2007). Long-range distance determinations in biomacromolecules by EPR spectroscopy. Q. Rev. Biophys. *40*, 1–53.

Schleiff, E., and Becker, T. (2011). Common ground for protein translocation: access control for mitochondria and chloroplasts. Nat. Rev. Mol. Cell Biol. *12*, 48–59.

Schleiff, E., Soll, J., Sveshnikova, N., Tien, R., Wright, S., Dabney-Smith, C., Subramanian, C., and Bruce, B.D. (2002). Structural and guanosine triphosphate/diphosphate requirements for transit peptide recognition by the

cytosolic domain of the chloroplast outer envelope receptor, Toc34. Biochemistry *41*, 1934–1946.

Schleiff, E., Soll, J., Küchler, M., Kühlbrandt, W., and Harrer, R. (2003). Characterization of the translocon of the outer envelope of chloroplasts. J. Cell Biol. *160*, 541–551.

Sommer, M.S., and Schleiff, E. (2009). Molecular interactions within the plant TOC complex. Biol. Chem. *390*, 739–744.

Sommer, M.S., Daum, B., Gross, L.E., Weis, B.L., Mirus, O., Abram, L., Maier, U.G., Kühlbrandt, W., and Schleiff, E. (2011). Chloroplast Omp85 proteins change orientation during evolution. Proc. Natl. Acad. Sci. USA *108*, 13841–13846.

Spindler, P.E., Zhang, Y., Endeward, B., Gershernzon, N., Skinner, T.E., Glaser, S.J., and Prisner, T.F. (2012). Shaped optimal control pulses for increased excitation bandwidth in EPR. J. Magn. Reson. *218*, 49–58.

Spindler, P.E., Glaser, S.J., Skinner, T.E., and Prisner, T.F. (2013). Broadband inversion PELDOR spectroscopy with partially adiabatic shaped pulses. Angew. Chem. Int. Ed. Engl. *52*, 3425–3429.

Stark, H., Rodnina, M.V., Wieden, H.J., van Heel, M., and Wintermeyer, W. (2000). Large-scale movement of elongation factor G and extensive conformational change of the ribosome during translocation. Cell *100*, 301–309.

Sun, Y.J., Forouhar, F., Li, H., Tu, S.L., Yeh, Y.H., Kao, S., Shr, H.L., Chou, C.C., Chen, C., and Hsiao, C.D. (2002). Crystal structure of pea Toc34, a novel GTPase of the chloroplast protein translocon. Nat. Struct. Biol. *9*, 95–100.

Wilden, B., Savelsbergh, A., Rodnina, M.V., and Wintermeyer, W. (2006). Role and timing of GTP binding and hydrolysis during EF-G-dependent tRNA translocation on the ribosome. Proc. Natl. Acad. Sci. USA *103*, 13670–13675.

Wittinghofer, A., and Vetter, I.R. (2011). Structure-function relationships of the G domain, a canonical switch motif. Annu. Rev. Biochem. *80*, 943–971.

Yang, Z. (2008). Cell polarity signaling in Arabidopsis. Annu. Rev. Cell Dev. Biol. *24*, 551–575.

Yoshida, Y., Miyagishima, S.Y., Kuroiwa, H., and Kuroiwa, T. (2012). The plastid-dividing machinery: formation, constriction and fission. Curr. Opin. Plant Biol. *15*, 714–721.

Yuksel, B., and Memon, A.R. (2009). Legume small GTPases and their role in the establishment of symbiotic associations with Rhizobium spp. Plant Signal. Behav. *4*, 257–260.

